

Full length article

Cold-formed stainless steel beams with single web hole at elevated temperatures

Andy Prabowo^a, Yuner Huang^{b,*}, Ben Young^c

^a Department of Civil Engineering, Universitas Tarumanagara, Jakarta, Indonesia

^b School of Engineering, University of Edinburgh, Scotland, United Kingdom

^c Department of Civil and Environmental Engineering, The Hong Kong Polytechnic University, Hong Kong, China

ARTICLE INFO

Keywords:

Cold-formed stainless steel
Direct strength method
Elevated temperatures
Perforated beams

ABSTRACT

Steel structures are often used in buildings due to their advantage in weight-to-strength ratio. However, their structural capacity deteriorates in fire as the temperature of the structures rises. Investigation of cold-formed stainless steel (CFSS) structures at elevated temperatures is still limited, especially for rectangular hollow section (RHS) beams having a single web hole in the mid-span (perforated web). Therefore, a numerical investigation was conducted to evaluate the current design provisions to calculate the strength of such beams at elevated temperatures ranging from 22 - 900 °C. A total of 400 specimens of stainless steel grades austenitic (EN 1.4301) and lean duplex (EN 1.4162) were considered. The investigation used finite element analysis (FEA) to simulate the behaviour of RHS beams with perforated web under pure bending. The finite element (FE) model was validated against a series of experimental results available in literature. The comparison between flexural strengths obtained from FEA with design values calculated from the current design rules showed that the design rules are conservative. However, they are not always reliable and safe for RHS beams without and with a perforated web for the two material grades at elevated temperatures. In this study, only the design rules specified by Eurocode 3 are shown to be reliable and safe.

1. Introduction

Cold-formed stainless steel (CFSS) has been increasingly used in various structural applications [1]. Various grades of stainless steel (SS) are available, which brings a wide range of options for construction. These grades generally have considerable strength and ductility with corrosion resistance, which make the use of SS favourable, especially in harsh environmental conditions [2]. However, CFSS structures experience strength deterioration when exposed to fire, similar to other steel materials.

Investigation of CFSS structures at elevated temperatures has recently gained researchers' attention. Finite element (FE) simulations were utilised to study the behaviour of structures at elevated temperatures. For example, Huang et al. [3] studied the behaviour of CFSS beam-columns fabricated from austenitic (EN 1.4301), duplex (1.4462), and lean duplex (1.4162) SS. Another study by Huang and Young [4] performed a series of numerical simulations for CFSS lean duplex (EN 1.4162) SHS/RHS beams. Separately, Huang and Young [5] also investigated the behaviour of CFSS lean duplex SHS/RHS columns. More

recently, Yan and Gernay [6] investigated the local buckling capacity of SHS/RHS columns for both carbon and stainless steel. An experimental investigation of the behaviour of I-section columns was recently conducted by Xing et al. [7]. These investigations evaluated the current design methods in the structural design specifications, showing that the existing design specifications do not always meet the minimum safety requirements. Furthermore, recent studies conducted by Quan and Kucukler [8], and Xing et al. [9,10] have focused on stainless steel SHS/RHS, I-sections and plates at elevated temperatures. The studies have covered a wide range of cross-section behaviour under pure axial compression, pure bending, combined axial compression and bending as well as combined bending and shear applicable to closed and open sections. It is shown that the proposed design rules in the studies are statistically safe and reliable.

The investigations of the behaviour of CFSS structures, especially those that relied on numerical simulation, required well-represented material properties to include material nonlinearity. Material properties of CFSS sections fabricated from austenitic grade were obtained by Chen and Young [11] and Gardner et al. [12]. Chen and Young [11]

* Corresponding author.

E-mail address: yuner.huang@ed.ac.uk (Y. Huang).

<https://doi.org/10.1016/j.tws.2023.111321>

Received 24 May 2023; Received in revised form 22 September 2023; Accepted 30 October 2023

Available online 18 November 2023

0263-8231/© 2023 The Author(s). Published by Elsevier Ltd. This is an open access article under the CC BY license (<http://creativecommons.org/licenses/by/4.0/>).

have proposed a stress-strain relationship model based on the test results of austenitic (EN 1.4301) and duplex (1.4462) SS rectangular hollow sections. Gardner et al. [12] proposed their elevated temperatures material model for austenitic SS, and claimed that their model had less complexity and better accuracy than the provisions in Eurocode 3 Part 1.2 [13]. Furthermore, Huang and Young [14] conducted a study on lean duplex SS. The material models from these two studies [11,14] were adopted by Huang et al. [3] to carry out numerical investigation on the design of CFSS structures at elevated temperatures. Refinements on the material model of CFSS at elevated temperatures were investigated by Fan et al. ([15] and [16]).

Similar to carbon steel (CS) members, SS members can be fabricated from hot-finished or cold-formed processes. Those fabricated from the cold-formed process are significantly faster and relatively cheaper [17] compared to hot-finished products. Currently, there are at least three international design specifications available for CFSS structures at ambient temperature, such as ASCE [18], EC3 Part 1.4 [19], and AS/NZS 4673 [20]. However, the structural design at elevated temperatures has not been addressed explicitly in ASCE [18]. Structural design for stainless steel structures using European Code EC3 Part 1.4 should be complemented by EC3 Part 1.2 [13] when the structure is subjected to elevated temperatures. The provisions in ASCE [18] are mainly based on the AISI [21] that was developed for carbon steel. The design provision for structural beams with a web perforation in ASCE are similar to AISI, except on the calculation of nominal flexural strength due to interaction of local and global buckling. Therefore, further research is needed to evaluate the suitability of these design rules for stainless steel beams with a web perforation at elevated temperatures.

Recently, Chen et al. [22] reported eighteen test results of perforated RHS beams fabricated from cold-formed ferritic SS (EN 1.4003). The measured yield strength of the specimens ranged from 410.4 MPa to 491.4 MPa. The web hole diameters ranged from 20% to 90% of the flat depth of the sections. The test setup is shown in Fig. 1. All the specimens failed in either flexural or combined local and flexural buckling mode. In addition to the experimental tests, Chen et al. [22] performed a numerical simulation of perforated RHS using FEA. The numerical model was validated with the test results. A comparison between the flexural strengths obtained from the tests and FEA is summarised in Table 1. Another study on the RHS perforated beams was conducted by Feng et al. [23], but the specimens were fabricated from aluminium alloy. It shall be noted that these investigations [22,23] were conducted at ambient temperature. Hence, the behaviour of such structures at elevated temperatures remains unknown.

The literature review shows a lack of attention on the behaviour of RHS beams with a web perforation at elevated temperatures. Therefore, this study aims to assess the suitability and the applicability of the current design rules for CFSS RHS beams with a web hole at elevated temperatures. Five design rules for calculating the flexural strength of CFSS RHS, based on the current international specifications [18,19,20,13] and a recent study [22], were evaluated based on the 400 FEA results obtained from this study. FE model was developed based on the

validated model presented in Chen et al. [22]. The investigation was applied to the two grades of SS, namely austenitic (EN 1.4301) and lean duplex (EN 1.4162), which have some differences in strength and ductility. The austenitic stainless steel is widely used in construction, while lean duplex stainless steel demonstrates high strength-to-cost ratio with excellent corrosion resistance [2]. The temperature variation considered in this study ranges from 22 - 900 °C.

2. Finite element model

2.1. FE model at ambient temperature

FE model of perforated RHS beams in this study was developed based on the model presented in Chen et al. [22], as shown in Fig. 2. The FE model was built in ABAQUS [24] using S4R shell elements, having four nodes and double curvature with reduced integration. The flat part of RHS had a mesh size of 7 mm × 7 mm, while the corner part was partitioned by five elements. A finer mesh was applied to the surrounding of the hole. Material properties reported in Chen et al. [22] were used in the FE model. The stress-strain values obtained from the coupon test were converted into true stress-logarithmic plastic strain values using Eqs (1) and (2).

$$\sigma_{true} = \sigma(1 + \epsilon) \quad (1)$$

$$\epsilon_{true,pl} = \ln(1 + \epsilon) - \sigma_{true}/E \quad (2)$$

where σ and ϵ are the stress and strain determined from the coupon tests, respectively, and E is the elastic modulus of the material being considered. Geometric imperfection was not considered in this study since the effect was insignificant to the FEA results for beams. The residual stress was also not incorporated into the model, similar to the FEA of cold-formed lean duplex SS beams at elevated temperatures performed by Huang and Young [4].

The two supports and the two loading points of the test setup were represented by four reference points (RP-1, RP-2, RP-3, and RP-4), as shown in Fig. 2. Degree of freedom (DOF) of the boundary conditions was consistent with the tests as shown in Fig. 1 and Fig. 3. RP-1 and RP-2 were defined for loading assignment by setting the target displacement. These two reference points were free to displace vertically but were restrained against the torsional DOF. RP-3 acted similarly to a roller, while RP-4 acted similarly to a pin. These four reference points were used as the master node that rigidly constrained all parts strengthened by the steel plate (L3 as shown in Fig. 3) in the tests. The FE model was analysed using static RIKS with geometric nonlinearity included to consider large deformation analysis. The accuracy of the FE model was evaluated by comparing the moment capacity obtained from tests (M_{Test}) and the FE model (M_{FEA}), as summarised in Table 1. Fig. 4 shows the moment versus rotation curves obtained from the test and FEA for specimen 60×40×4D50. The comparison of failure mode obtained from the test and FEA for specimen 80×60×4D80 is presented in Fig. 5. It is shown that the FEA results closely predicted the test results.

2.2. FE model at elevated temperatures

The validated FE model is used in this study to investigate the flexural strength of perforated RHS beams fabricated from austenitic and lean duplex SS at various temperatures, ranging from 22 °C to 900 °C. The heat transfer mechanism was assumed uniform due to the thermal conductivity of stainless steel material. The material properties of the FE model at elevated temperatures were calculated from the stress-strain relationship proposed by Chen and Young [11] and Huang and Young [14], for austenitic and lean duplex SS, respectively. The same relationship was used by Huang et al. [3] in their study on the structural performance of CFSS beam-columns at elevated temperatures. Table 2 shows the key mechanical properties obtained from the references [11,

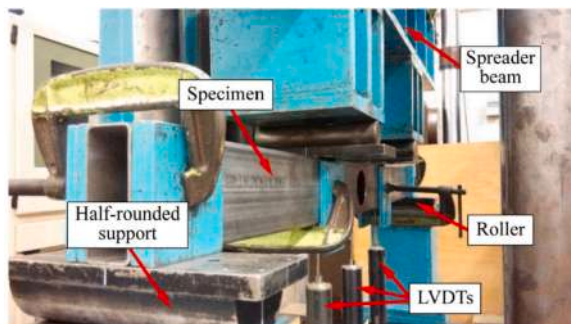


Fig. 1. Test setup of perforated RHS beam [22].

Table 1
Comparison between experimental and FEA results at ambient temperature [22].

Specimen ($d \times b \times t$)	D/h (%)	M_{Test} (kNm)	M_{FEA} (kNm)	M_{Test}/M_{FEA}	κ_{Test} (10^{-4} mm^{-1})	κ_{FEA} (10^{-4} mm^{-1})	$\kappa_{Test}/\kappa_{FEA}$
60 × 40 × 4	0	7.59	7.41	1.02	4.92	5.13	0.96
	20	7.54	7.40	1.02	4.89	5.12	0.95
	50	7.12	6.76	1.05	2.11	3.00	0.70
	80	6.23	6.21	1.00	1.52	1.67	0.91
80 × 60 × 4	0	14.49	13.90	1.04	3.23	3.10	1.04
	20	14.43	13.73	1.05	3.18	3.10	1.03
	50	13.67	13.38	1.02	1.32	1.58	0.83
	50(r)	13.88	13.38	1.04	1.41	1.58	0.89
	80	12.28	11.95	1.03	0.96	1.12	0.85
100 × 40 × 2	0	8.32	7.83	1.06	1.22	2.35	0.52
	20	8.2	7.88	1.04	1.28	1.82	0.71
	50	7.40	7.22	1.02	0.82	0.94	0.87
	50(r)	7.57	7.22	1.05	0.84	0.94	0.89
	80	6.15	5.83	1.05	0.66	0.66	1.00
120 × 80 × 3	0	21.63	20.16	1.07	0.81	1.21	0.67
	20	21.83	20.14	1.08	0.80	1.21	0.66
	50	20.26	19.05	1.06	0.54	1.13	0.48
	80	17.75	16.04	1.11	0.47	0.47	0.98
			Mean		1.05		
		COV		0.019			0.204

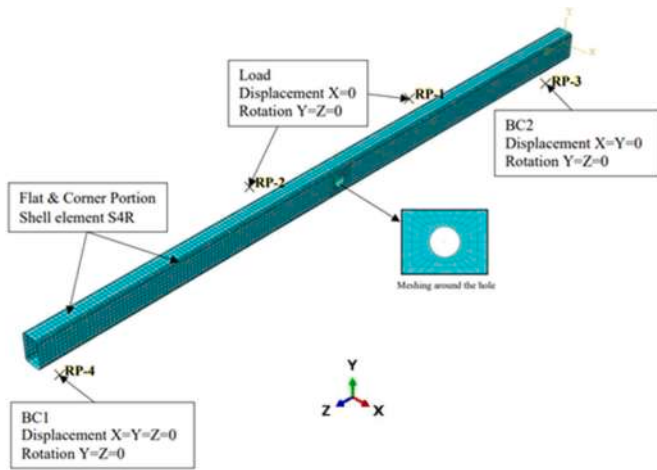


Fig. 2. Finite element model of perforated RHS beam.

[14] at five different temperatures. All the stress-strain values from the proposed relationship were converted using Eqs. (1) and (2) to model the plastic behaviour of the CFSS beams with single web hole at elevated temperatures in this study. The elastic properties at elevated temperatures were the reduced Young’s modulus obtained from the references [11,14] and the Poisson ratio value. The other setup on the FE model at elevated temperatures is the same as those at ambient temperature.

3. Parametric study

An extensive parametric study was conducted for 400 FE specimens

built in ABAQUS [24]. There are 200 specimens with austenitic (EN 1.4301) and lean duplex (EN 1.4162) SS grades, respectively. The specimen cross-sections were determined by varying the web slenderness (h/t) range, where h is the flat depth and t is the thickness of the RHS. Notations of the cross-section are defined in Fig. 3, where d is the overall depth and b is the overall width of the RHS. There were eight cross-section variations with h/t ranging from 10.8 to 246.7. All sections were subjected to major axis bending, except for 380×570×2 and 380×570×4 subjected to minor axis bending. The hole diameters in the perforated sections were determined as 20%, 50%, 70%, and 90% of the flat depth (h). The non-perforated section was included to study the strength reduction pattern. The temperature variations for austenitic specimens were slightly different from the lean duplex specimens, as

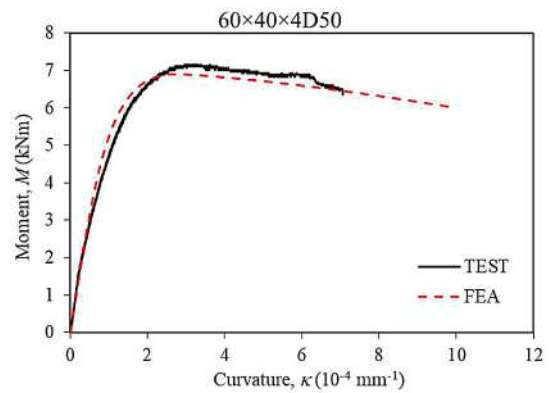


Fig. 4. Moment versus curvature curves obtained from the test and FEA for specimen 60×40×4D50.

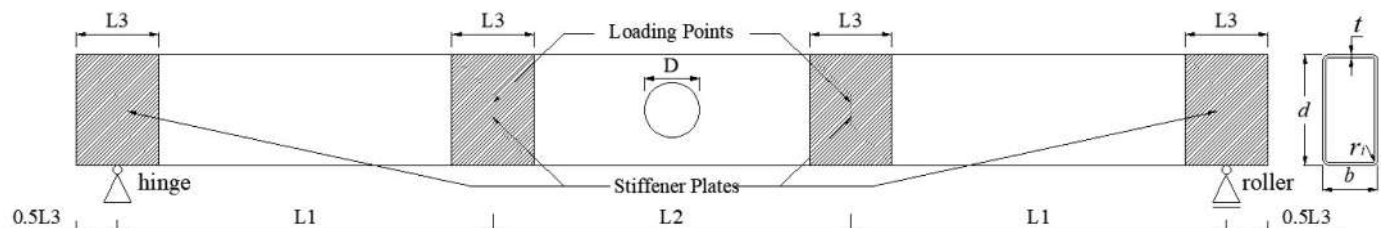


Fig. 3. Dimensions of specimen.



Fig. 5. Comparison of failure mode obtained from the test and FEA for specimen 80×60×4D80.

Table 2
Material properties of cold-formed stainless steel RHS at various temperatures [11,14].

Grade	T (°C)	E _T (GPa)	σ _{0.2,T} (MPa)	σ _{2,T} (MPa)	σ _{u,T} (MPa)	ε _u (%)
Austenitic (EN 1.4301)	22	187	398	452	709	60.6
	320	194	278	330	497	21.8
	550	168	237	287	459	19.3
	660	161	208	261	333	11.1
	870	84	72	71.9	72.1	11.9
Lean duplex (EN 1.4162)	24	199	682	802	828	21.5
	300	159	519	666	706	14.4
	500	131	384	497	623	14.0
	700	102	192	257	257	3.1
	900	40	54	67	67	2.2

Note: σ_u is taken as the maximum stress value in the stress-strain curve.

also studied by Huang et al. [3]. The aforementioned parameter variations are summarised in Table 3. The length of the specimens was consistent with those specimens investigated by Chen et al. [22], as shown in Fig. 3. The moment span (L2) was 410 mm and the shear span (L1) was 390 for specimens (d × b) 60×40 and 120×80. For the specimens larger than 120×80, the L2 and the L1 were 1400 mm.

Each FE specimen has a unique label to distinguish the grade of SS, cross-section sizes, percentage of hole diameter, and temperature. For instance, labels of L300×120×2D50T300 and A380×570×4D0T550 have the following meaning:

- The first letter signifies the grade of SS (“L” = lean duplex EN 1.4162, “A” = austenitic EN 1.4301).
- The next set of digits indicates the “d”, “b”, and “t”, respectively. For example, 300×120×2 means d = 300, b = 120, and t = 2.
- The following letter and digit indicate the hole diameter variation: “D50” is used for specimens with a web hole diameter of 50% h, and “D0” is used for specimens without a web hole.
- Finally, the last letter and number identify the temperature variations: “T300” indicates the temperature of 300 °C, and “T550” indicates the temperature of 550 °C.

Fig. 5 shows the typical failure mode of the RHS beams with a single web hole under pure bending, which is combined local and flexural buckling. In addition, the FEA results of moment-curvature diagrams are

Table 3
Parameter variations in the parametric study.

Parameters	Austenitic & Lean duplex
Sections (d × b × t)	60×40×4, 120×80×3, 300×120×4.5, 380×286×2, 380×152×1.5, 380×380×4, 380×570×4, 380×570×2
Web slenderness (h/t)	10.8 – 246.7
Inner radius to thickness ratio (r _i /t)	0.9 – 2.3
Hole diameter to web depth ratio (D/h)	0, 20%, 50%, 70%, 90%
Elevated temperatures (°C)	22, 320, 550, 660, 870 (Austenitic) 24, 300, 500, 700, 900 (Lean duplex)

shown in Figs. 6-9, describing the behaviour of the RHS beams at various temperatures. The curvature was calculated using the Eq. (7) in Chan and Gardner [25]. It can be observed that the stiffness decreases as the temperature increases. The deflection of the specimens with the same hole diameter were similar up to the temperature 500 °C, but the deflection gradually decreased as the temperature beyond 500 °C for the lean duplex SS beams.

The flexural strengths of 400 specimens obtained from the FEA are presented in Table 4, which were used to evaluate the current strength predictions from the design specifications. The moment reduction due to perforation calculated by comparing the moment strength of specimens with and without a web hole were depicted in Figs. 10 and 11. The moment reductions of different web hole diameters were plotted against the slenderness factor of local buckling (λ_l) for the two grades of SS and at various elevated temperatures. On average, the moment reduction values generally decreased when the λ_l increased, but at an inconsistent rate for different temperatures. It was also found that the strength reduction for specimens with D = 20% h could be neglected since the reductions were less than 10% of the moment capacity without hole, and minor strength enhancements were observed on lean duplex SS specimens.

4. Reliability assessment

A thorough reliability assessment was carried out to evaluate the safety level of the existing design rules in the current specifications (ASCE [18], AS/NZS [20], EC3 Part 1.4 [19], and EC3 Part 1.2 [13]) and a newly proposed design rule by Chen et al. [22]. Two kinds of assessment were implemented, which involved the calculation of the reliability index (β_o) and the safety evaluation criteria proposed by Kruppa [26], specifically for the fire resistance design of structures. These assessments were also carried out in the study of beam-column design at elevated temperatures by Huang et al. [3].

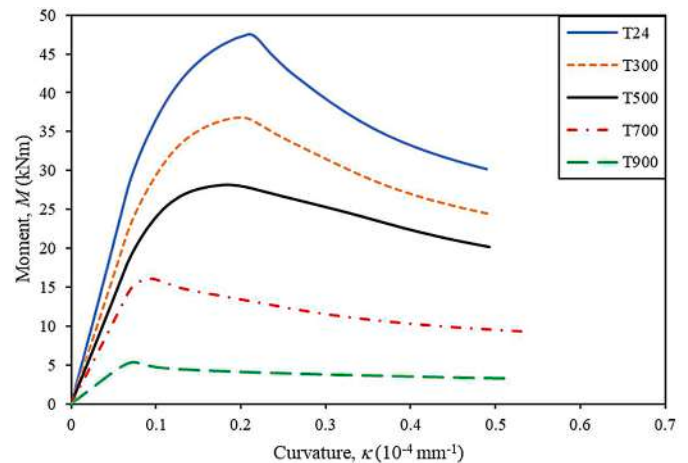


Fig. 6. Moment versus curvature curves for L300×120×2D20 at various temperatures.

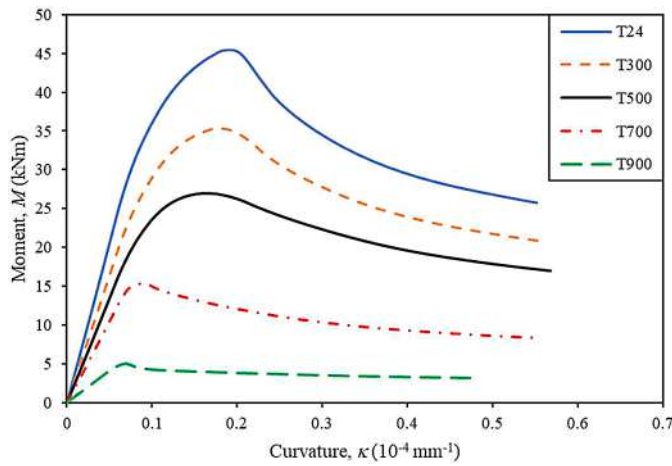


Fig. 7. Moment versus curvature curves for specimen L300×120×2D50 at various temperatures.

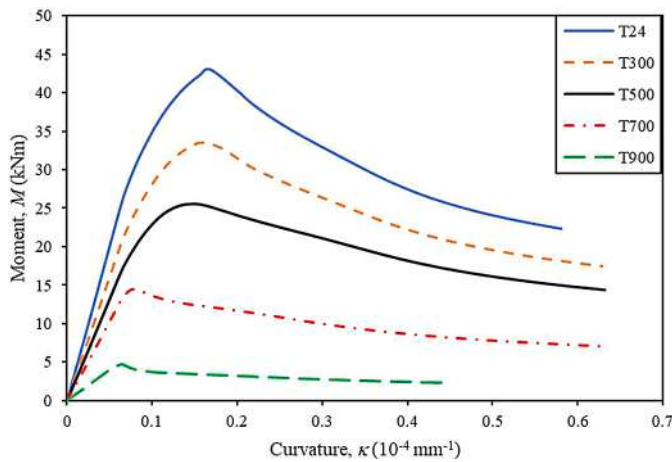


Fig. 8. Moment versus curvature curves for specimen L300×120×2D70 at various temperatures.

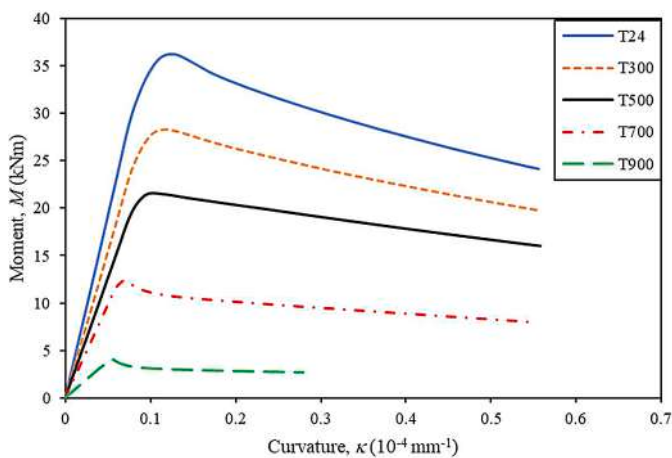


Fig. 9. Moment versus curvature curves for specimen L300×120×2D90 at various temperatures.

4.1. Reliability index

The values of the reliability index (β_o) were obtained from the reliability analysis procedure prescribed in Chapter 11 of ASCE [18]. The β_o

values of all design rules were assessed using the same approach to compare the safety level of different specifications directly. ASCE [18] demands a minimum β_o of 2.5 to conclude that the design rule being considered is probabilistically safe and reliable for structural members. The load combination and resistance factor (ϕ), named as uncertain variables in the β_o calculation, were taken from the specifications that considered in this study. Therefore, four load combinations based on Dead Load (DL) and Live Load (LL) contributions were used: 1.2DL+1.6LL (for ASCE [18] and Chen et al. [22]), 1.2DL+1.5LL for (AS/NZS [20]), and 1.35DL + 1.5LL (for the two EC3 codes [19,13]). These load combinations were used to determine C_ϕ values based on Meimand and Schafer [27]. The ϕ values from different specifications can be seen in Table 5 and Table 6. It should be noted that the ϕ values from the two EC3 codes [19,13] were reciprocal to γ_{M1} and γ_{Mf} . The formula of β_o can be shown in Eq. (3).

$$\beta_o = \frac{\ln(C_\phi M_m F_m P_m / \phi)}{\sqrt{V_M^2 + V_F^2 + C_p V_P^2 + V_Q^2}} \tag{3}$$

Values of other parameters in Eq. (3) were guided in the specifications, and a few of them were distinguished by the grade of SS. Those include the mean values of material factor M_m of yielding limit states for austenitic and duplex families were 1.25 and 1.1, respectively, while the corresponding coefficients of variation (COV) V_M were 0.1 and 0.05, respectively. The mean value of fabrication factor F_m and the corresponding COV V_F were 1.0 and 0.05, respectively, regardless of the grade of SS. In addition, the correction factor C_p that accounts for the influence of small number of data was determined using Eqs. (11-4) in the ASCE Specification [18], and the coefficient of variation of load effect V_Q was 0.21. Lastly, the P_m and V_P were obtained from the mean and COV values of the ratio between strengths predicted by FEA and design rules. Results of the reliability analyses are collected in Tables 5 and 6.

4.2. Safety evaluation criteria of Kruppa's proposal

The safety evaluation using criteria proposed by Kruppa [26] was performed by Huang et al. [3] for design of beam-columns at elevated temperatures. The criteria were to ensure that the strength obtained from the test or FEA was always more conservative than the predicted strength calculated from a design rule. The structural safety in the fire resistance design can be assured if these three criteria are met:

- The mean value of the FEA-to-strength prediction ratio (P_m) is greater than one.
- The proportion of the FEA-to-strength prediction ratio less than one (% ratio < 1) shall be lower than 20%.
- The smallest value of the FEA-to-strength prediction ratio shall be 0.85.

The safety evaluation results for all the design rules based on the above criteria are presented in Tables 5 and 6.

5. Evaluation of design rules

5.1. General

Design rules to obtain the flexural strength of CFSS beams, particularly for RHS, at ambient temperature can be found in ASCE [18], AS/NZS [20], and EC3 Part 1.4 [19]. Amongst these three specifications, only ASCE [18] has a specific design rule for RHS beams with and without a web hole using Direct Strength Method (DSM). However, ASCE [18] also allows an alternative design rule using Effective Width Method (EWM), which is a more traditional design method than DSM. The EWM is the only method recommended by AS/NZS [20] and EC3 Part 1.4 [19] since these two specifications were written when the DSM had not been proposed. Although the DSM and EWM have been

Table 4
Flexural strength values (kNm) obtained from FEA.

Cross-section			T (°C)	Austenitic (EN 1.4301)					T (°C)	Lean duplex (EN 1.4162)				
d (mm)	b (mm)	t (mm)		D0	D20	D50	D70	D90		D0	D20	D50	D70	D90
60.07	40.24	3.87	22	7.1	6.9	6.2	5.8	5.4	24	10.3	10.1	9.4	8.9	8.1
			320	5.8	5.6	5.0	4.6	4.3	300	8.8	8.5	7.8	7.4	6.7
			550	5.4	5.2	4.6	4.2	3.9	500	7.7	7.5	6.7	6.2	5.7
			660	4.2	4.1	3.7	3.5	3.2	700	3.1	3.1	2.9	2.7	2.5
			870	0.9	0.9	0.9	0.9	0.8	900	0.8	0.8	0.8	0.7	0.7
120.02	80.3	2.89	22	18.5	18.4	17.6	15.5	13.1	24	30.3	30.3	29.0	26.5	21.2
			320	13.3	13.3	12.9	11.4	9.3	300	23.4	23.4	23.0	21.2	14.9
			550	11.4	11.4	11.0	9.7	7.9	500	18.0	18.0	17.7	16.1	11.3
			660	10.5	10.5	10.1	9.0	7.3	700	9.0	9.1	8.9	7.8	6.3
			870	3.2	3.2	3.0	2.7	2.3	900	2.5	2.5	2.4	2.2	1.8
300	120	2	22	32.2	31.4	29.9	28.2	24.1	24	48.7	47.3	45.4	43.0	36.2
			320	26.4	26.0	24.5	23.4	19.4	300	37.9	36.8	35.4	33.5	28.3
			550	22.8	22.6	21.4	20.1	17.1	500	28.9	28.1	27.0	25.5	21.5
			660	19.3	19.1	18.2	17.1	14.5	700	16.3	16.0	15.4	14.4	12.3
			870	10.0	9.5	8.1	7.8	6.2	900	5.4	5.4	5.0	4.8	4.0
380	286	2	22	47.1	46.4	44.5	43.2	36.4	24	73.4	68.5	67.4	65.4	54.1
			320	40.1	37.3	36.0	33.6	29.2	300	57.0	53.4	52.3	50.3	42.2
			550	34.4	32.1	31.0	28.4	25.1	500	43.8	40.8	39.5	38.4	32.3
			660	28.0	27.8	26.0	25.0	21.7	700	25.3	23.7	23.0	21.7	18.7
			870	13.1	12.1	11.5	10.7	10.7	900	8.1	7.5	7.2	6.5	5.7
380	152	1.5	22	26.8	26.7	26.6	23.9	20.3	24	40.1	39.4	37.5	36.0	35.7
			320	21.8	21.1	20.4	18.7	15.9	300	31.3	30.6	29.0	28.0	24.6
			550	18.8	18.3	18.2	16.1	13.7	500	23.7	23.3	22.2	21.4	18.7
			660	15.8	15.4	14.5	13.9	11.8	700	13.4	13.3	12.7	12.0	10.3
			870	7.2	6.8	6.8	6.0	5.7	900	4.4	4.2	4.2	3.8	3.2
380	380	4	22	169.6	167.5	157.5	144.4	128.2	24	290.5	289.5	274.9	219.2	192.7
			320	135.6	131.5	123.2	112.7	111.9	300	226.1	226.1	215.6	197.5	178.2
			550	122.0	115.0	104.6	97.1	81.6	500	174.2	174.5	142.8	134.8	114.2
			660	115.3	106.0	104.4	85.3	73.2	700	110.3	109.3	104.8	86.6	84.8
			870	43.1	41.7	38.8	35.7	35.6	900	33.8	33.7	32.5	30.8	25.7
380	570	4	22	196.5	195.1	169.5	153.5	136.9	24	283.8	282.5	253.7	230.8	209.8
			320	161.3	160.3	133.2	123.8	107.0	300	220.8	221.2	197.0	184.1	164.4
			550	139.2	138.4	115.2	106.7	91.9	500	171.0	169.9	150.7	141.3	125.2
			660	118.9	107.4	100.2	91.9	79.3	700	101.1	100.4	85.3	79.7	68.9
			870	50.9	50.4	43.0	38.9	33.7	900	32.5	32.2	27.0	24.7	21.4
380	570	2	22	54.4	54.4	53.0	52.6	47.9	24	78.0	77.9	77.4	75.6	69.3
			320	44.6	44.6	43.8	42.7	38.7	300	60.8	61.4	60.4	59.1	54.4
			550	38.5	38.4	37.6	36.9	33.3	500	47.0	47.3	45.6	45.6	42.2
			660	33.1	33.0	32.7	31.8	28.8	700	27.8	28.0	27.7	26.9	24.4
			870	14.9	14.8	14.6	14.0	12.3	900	8.9	9.0	8.7	8.6	7.7

developed for structural design at ambient temperatures, the two methods may be extended for structures at elevated temperatures using the yield strength at ambient temperature ($\sigma_{0.2,T}$) as the strength limit, where the reduced yield strength was used in calculating the flexural strength due to elevated temperatures.

In this study, the DSM in ASCE [18] and the EWM in AS/NZS [20] and EC3 Part 1.4 [19] were evaluated. A recent modification on the DSM equation proposed by Chen et al. [22] for ferritic SS grade was also evaluated for its applicability to the austenitic and lean duplex SS grades. In addition, the design rule based on the fire resistance consideration recommended by EC3 Part 1.2 was also evaluated to broaden the scope of the evaluation. Details on the design rules are explained below.

5.2. ASCE specification

According to Section 6.1 of ASCE [18], the flexural strength of non-perforated RHS beams shall be taken from the minimum value of M_{ne} (yielding and global buckling) calculated from Section 6.2 and M_{nl} (local buckling interacting with yielding and global buckling) in Section 6.3 of ASCE [18]. The M_{ne} should be equal to the yielding capacity (M_y) of RHS beams since lateral-torsional buckling normally does not occur to RHS beams. The M_y is calculated from the elastic modulus of cross-sections times the yield strength limit. The DSM equations are included in Section 6.3 of ASCE [18], which considers the failure interaction between local and global buckling. In summary, the moment capacity of non-perforated RHS beams (sections with $D = 0$) using DSM

equations can be calculated from Eqs (4)-(7). The M_{cr1} (critical-elastic local buckling moment) in Eq. (7) was obtained from the CUFSM [28] calculation.

$$M_{ASCE} = \min(M_{ne}, M_{nl}) \tag{4}$$

For $\lambda_l \leq 0.667$, $M_{nl} = M_{ne}$ (5)

For $\lambda_l > 0.667$, $M_{nl} = \left(\frac{1}{\lambda_l^{0.8}} - \frac{0.2}{\lambda_l^{1.6}} \right) M_{ne}$ (6)

$$\lambda_l = \sqrt{M_{ne}/M_{cr1}} \tag{7}$$

The flexural strength for perforated beams (sections with $D > 0$) using the DSM approach was calculated based on Moen and Schafer [29] proposal, which has been adopted by AISI [21]. The proposal was developed for cold-formed CS structures, while it has recently been applied by Chen et al. [22] for CFSS structures. In the DSM for perforated sections, the M_{nl} shall be the lowest value between M_{ne} and M_{ynet} (the yield moment based on the net cross-section) when λ_l smaller than the limit (0.667 for CFSS and 0.776 for cold-formed CS). In order to obtain M_{cr1} for perforated sections, specific procedures in using CUFSM mentioned by Moen and Schafer [29] were implemented in this study. The top corners of the cross-sections for perforated sections were restrained against translation in CUFSM, as recommended by Moen and Schafer [29]. Fig. 12 shows an example of the CUFSM calculation result using the recommended steps [29], exhibiting the local buckling mode

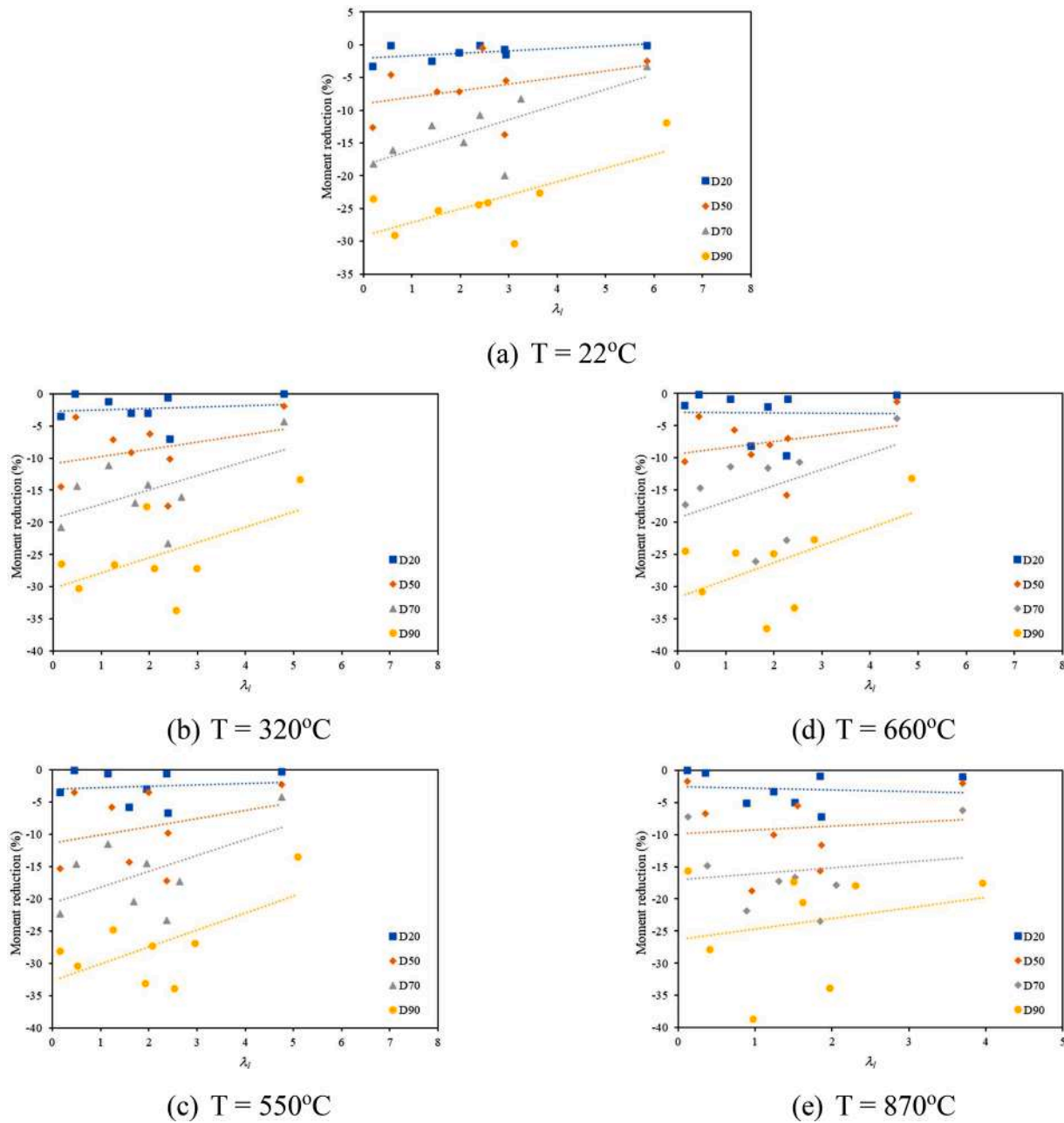


Fig. 10. Moment reduction of austenitic stainless steel specimens with the hole diameter of 20%, 50%, 70%, and 90% of flat web depth at elevated temperatures.

and the corresponding load factor that read from the signature curve. The x-axis of the graph represents the L_{crl} (local buckling half-wavelength), and the y-axis represents the M_{crl} in terms of load factor times M_y . After the signature curve has been obtained from CUFSM, the M_{crl} for a perforated section (M_{crlh}) is determined as follows:

- If $D < L_{crlh}$, the M_{crl} from the signature curve corresponding to $L_{crl} = D$ is taken as M_{crlh} .
- If $D > L_{crlh}$, the M_{crl} from the signature curve corresponding to $L_{crl} = L_{crlh}$ is taken as M_{crlh} .
- For all possibilities, the value of M_{crlh} shall not be larger than the M_{crlnh} (M_{crl} when the hole is not considered).

The flexural strengths obtained from FEA were compared with the predicted strengths obtained from ASCE [18]. Fig. 13 shows the values of M_{FEA}/M_{ASCE} for all specimens. The mean values and COV of M_{FEA}/M_{ASCE} for sections having $D = 0$ and $D > 0$ are presented Tables 5 and 6,

respectively. For sections with $D = 0$, the mean values of M_{FEA}/M_{ASCE} for the austenitic and lean duplex were above 1.2, with the COV values of at least 0.178. For sections with $D > 0$, the mean values of M_{FEA}/M_{ASCE} for the two grades of SS were above 1.1, with the minimum value of COV at 0.195. These results show that the ASCE [18] design rules are overly conservative, as the mean values were far above 1. The predicted strengths are also relatively scattered as the COV values are quite large.

Results from the reliability analysis show that the ASCE design rule of flexural strength for sections without a web hole is more reliable than that with a web hole. This is shown in Table 5 that the β_0 values are above 2.5, while the values were equal to or slightly lower than 2.5 in Table 6. Results from the safety evaluation using Kruppa's proposal are also shown in the two tables. The ASCE design rule for sections with $D = 0$ met all the safety criteria, but not for sections with $D > 0$. The first and second criteria of the proposal could be fulfilled as the strength ratio was above one, and the percentages of the strength ratio less than one were higher than 20%. However, the ASCE design rule for sections with $D >$

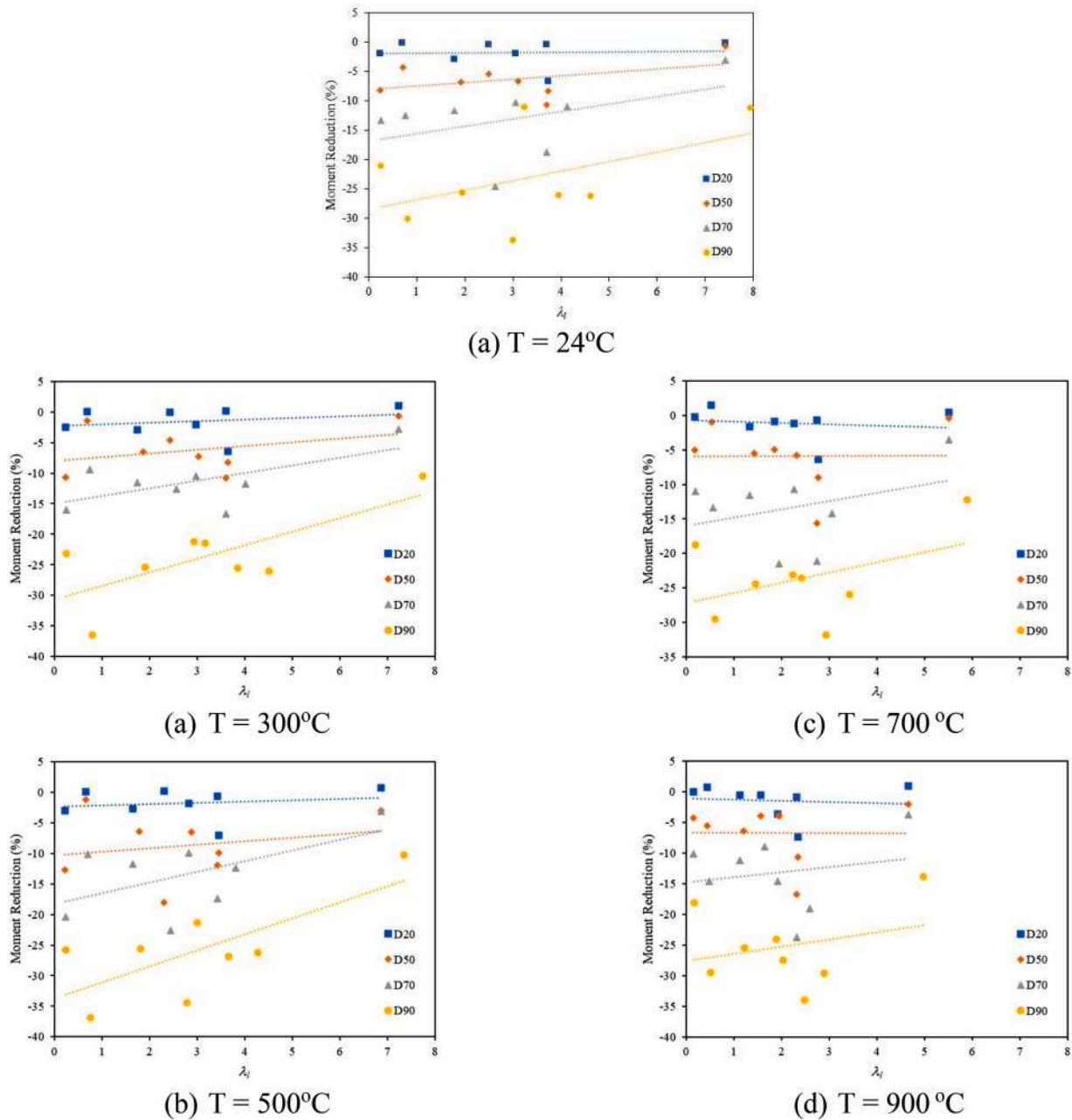


Fig. 11. Moment reduction of lean duplex stainless steel specimens with the hole diameter of 20%, 50%, 70%, and 90% of flat web depth at elevated temperatures.

0 failed to meet the third criterion since the lowest strength ratio was smaller than 0.85.

5.3. Modified DSM equations proposed by Chen et al. [22]

The modified DSM equations obtained from Chen et al. [22] study for ferritic beams are written as follows:

$$M_{DSM\#} = \min(M_{ne}, M_{nl}) \tag{8}$$

$$\text{For } \lambda_l \leq 0.776, M_{nl} = \left(1.5 - \frac{0.5}{0.776}\lambda_l\right)M_{ne} \tag{9}$$

$$\text{For } \lambda_l > 0.776, M_{nl} = \left(\frac{1}{\lambda_l^{0.8}} - \frac{0.15}{\lambda_l^{1.6}}\right)M_{ne} \tag{10}$$

The above equations were proposed based on the test and FEA results

of perforated and non-perforated RHS beams. The value of λ_l limit is the same as that used in AISI [21]. The calculation procedures for obtaining M_{cr1} which formulated by Moen and Schafer [29] to obtain the λ_l value was used. The applicability of the modified DSM equations has been assessed in this study for cold-formed austenitic and lean duplex SS beams.

The comparison between M_{FEA} and $M_{DSM\#}$ values is shown in Fig. 14, where the discrepancy between the flexural strengths was relatively small at the small values, and it became larger at the higher values. The mean values of $M_{FEA}/M_{DSM\#}$ for sections with $D = 0$ were greater than 1.10, with the highest COV value at 0.146, as shown in Table 5. For sections with $D > 0$, the mean values in Table 6 were much lower than those in Table 5, while the highest COV value of 0.150 was obtained. It can be inferred that the modified DSM equations offer less conservative and less scattered predictions than the DSM in the ASCE [18].

Similar to the evaluation results from ASCE [18], the β_o values listed in Table 5 exceeded 2.5, while not all β_o values listed in Table 6 exceeded

Table 5

Comparison between FEA results with nominal strengths predicted from design rules for cold-formed stainless steel RHS beams without a web hole (sections with $D = 0$).

	$\frac{M_{FEA}}{M_{ASCE}}$	$\frac{M_{FEA}}{M_{DSM\#}}$	$\frac{M_{FEA}}{M_{AS/NZS}}$	$\frac{M_{FEA}}{M_{EC3}}$	$\frac{M_{FEA}}{M_{EC3\#}}$
Austenitic (EN 1.4301)					
Number of data	40	40	40	40	40
Mean (P_m)	1.24	1.11	1.16	1.26	1.41
COV (V_p)	0.249	0.146	0.283	0.129	0.202
Resistance factor (ϕ)	0.90	0.90	0.9	0.91	1.00
Reliability index (β_o)	2.73	3.03	2.22	3.39	2.99
% ratio < 1	15%	30%	23%	0%	8%
Smallest ratio	0.93	0.90	0.81	1.00	0.89
Kruppa criteria	Passed	Failed	Failed	Passed	Passed
Lean duplex (EN 1.4162)					
Number of data	40	40	40	40	40
Mean (P_m)	1.23	1.14	1.17	1.32	1.43
COV (V_p)	0.178	0.115	0.199	0.086	0.210
Resistance factor (ϕ)	0.90	0.90	0.9	0.91	1.00
Reliability index (β_o)	2.87	2.97	2.39	3.53	2.68
% ratio < 1	2.5%	17.5%	20%	0%	8%
Smallest ratio	0.98	0.95	0.87	1.14	0.93
Kruppa criteria	Passed	Passed	Failed	Passed	Passed

Table 6

Comparison between FEA results with nominal strengths predicted from design rules for cold-formed stainless steel RHS beams with a web hole (sections with $D > 0$).

	$\frac{M_{FEA}}{M_{ASCE}}$	$\frac{M_{FEA}}{M_{DSM\#}}$	$\frac{M_{FEA}}{M_{AS/NZS}}$	$\frac{M_{FEA}}{M_{EC3}}$	$\frac{M_{FEA}}{M_{EC3\#}}$
Austenitic (EN 1.4301)					
Number of data	160	160	160	160	160
Mean (P_m)	1.12	0.99	1.17	1.22	1.34
COV (V_p)	0.252	0.150	0.207	0.152	0.189
Resistance factor (ϕ)	0.90	0.90	0.90	0.91	1.00
Reliability index (β_o)	2.46	2.61	2.69	3.18	2.93
% ratio < 1	42%	59%	18%	3%	9%
Smallest ratio	0.73	0.70	0.85	0.94	0.88
Kruppa criteria	Failed	Failed	Passed	Passed	Passed
Lean duplex (EN 1.4162)					
Number of data	160	160	160	160	160
Mean (P_m)	1.13	1.03	1.19	1.26	1.36
COV (V_p)	0.195	0.136	0.154	0.120	0.213
Resistance factor (ϕ)	0.90	0.90	0.90	0.91	1.00
Reliability index (β_o)	2.50	2.48	2.72	3.16	2.52
% ratio < 1	31%	49%	13%	3%	8%
Smallest ratio	0.76	0.74	0.89	0.98	0.87
Kruppa criteria	Failed	Failed	Passed	Passed	Passed

2.5. It means that the modified DSM equations are only reliable for sections without a web hole. Furthermore, the evaluation using the three criteria proposed by Kruppa [26] show that the modified DSM equations provide unsafe prediction results since there was always one criterion that could not be met. That criterion was either the total percentage of $M_{FEA}/M_{DSM\#} < 1$ or the lowest percentage of $M_{FEA}/M_{DSM\#}$, as shown in Tables 5 and 6.

Meanwhile, Figs. 15 and 16 present two DSM curves obtained from ASCE [18] and Chen et al. [22] design rules plotted with the ultimate strengths (M_u) obtained from FEA and normalised by M_{ne} values. The two curves were generally close to the normalised M_u . However, the one obtained from Chen et al. [22] design rule is more realistic than the ASCE [18] since a higher strength value than M_y was permitted for $\lambda_l \leq 0.776$. The ASCE [18] design rule is more conservative than the Chen et al. [22] design rule since it does not permit a higher strength than M_y for $\lambda_l \leq 0.667$.

5.4. AS/NZS standard

The flexural strength calculated based on AS/NZS [20] design rule ($M_{AS/NZS}$) was determined from the basis of initiation of yielding in the effective section, as specified in Clause 3.3.2.2. The value of $M_{AS/NZS}$ was obtained from Eq. (11), where S_e is the elastic modulus of the effective cross-section, and $\sigma_{0.2,T}$ is consistent with the temperature being considered. The effective cross-section properties were calculated using the effective width equations from Clause 2.2 of AS/NZS [20], with the yield stress and Young’s modulus varied depending on the reduced values. It should be noted that RHS without a web hole is composed of two stiffened elements at the flange and web. For perforated sections, the web is treated as unstiffened elements since the edge adjacent to the web hole is free to displace. These principles were also used for the effective width calculations in EC3 [19].

$$M_{AS/NZS} = S_e \sigma_{0.2,T} \tag{11}$$

The comparison between M_{FEA} and $M_{AS/NZS}$ obtained from a total of 400 specimens is presented in Fig. 17. The ratio of $M_{FEA}/M_{AS/NZS}$ for all specimens was also calculated, which had the mean and COV values as listed in Tables 5 and 6. In the two tables, the mean values were greater than 1.1, indicating that the AS/NZS [20] design rule is conservative. The COV values ranged from 0.154 to 0.283, which is considered to be relatively high. These values defined the four β_o values ranging from 2.22 to 2.72. It is observed that the AS/NZS [20] design rules were not reliable for the sections with $D = 0$ since its β_o value was smaller than 2.5, according to Table 5. In contrast, all β_o values in Table 6 exceeded 2.5. The AS/NZS [20] design rule could not meet the safety criteria proposed by Kruppa [26] since not all the criteria were fulfilled.

5.5. EC3 part 1.4

The flexural strength obtained from the EC3 Part 1.4 [19] (M_{EC3}) was determined using the procedure described in Section 5.2. The flexural strength was calculated by the effective section modulus (S_e) for Class 4 sections. The flexural strength of Class 3 sections was determined using the full elastic modulus (S_f), while Class 1 and 2 sections were based on the plastic modulus (Z). The highest class number between the web and flange shall be taken as the section classification. Reduced material properties were used for the classification of cross-sections at elevated temperatures. The flexural strength equations are shown in Eqs (12)-(14). In this study, the S_e was calculated based on the effective width equations prescribed by EC3 Part 1.5 [30], except for the reduction factor (ρ) that calculated from EC3 Part 1.4 [19].

$$M_{EC3} = S_e \sigma_{0.2,T} \text{ (for class 4 cross – sections)} \tag{12}$$

$$M_{EC3} = S_f \sigma_{0.2,T} \text{ (for class 3 cross – sections)} \tag{13}$$

$$M_{EC3} = Z \sigma_{0.2,T} \text{ (for class 1 or 2 cross – sections)} \tag{14}$$

Fig. 18 presents all the M_{FEA} values that were compared with M_{EC3} . The figure indicates that most of the M_{FEA} values were greater than M_{EC3} . The four mean values of M_{FEA}/M_{EC3} ranged from 1.22 to 1.32, which suggests that the EC3 [19] design rules are conservative for the specimens with and without a web hole fabricated from the two grades of SS. The COV values of M_{FEA}/M_{EC3} were smaller than $M_{FEA}/M_{AS/NZS}$ and M_{FEA}/M_{ASCE} , ranging from 0.086 to 0.152, noting that the EC3 Part 1.4 [19] design rules provide less scattered prediction results compared to ASCE (Section 5.2), Chen et al. (Section 5.3), and AS/NZS (Section 5.4). In addition, no β_o value smaller than 2.5 was observed for M_{FEA}/M_{EC3} in Tables 5 and 6, which demonstrates the reliability of EC3 Part 1.4 [19] design rules.

The EC3 Part 1.4 [19] design rules applied to the two grades of SS meet all the safety criteria proposed by Kruppa [26]. As shown in Table 5, all the M_{FEA}/M_{EC3} values for the section without a web hole were greater than 1.0 for both SS grades since the percentage of “ratio <

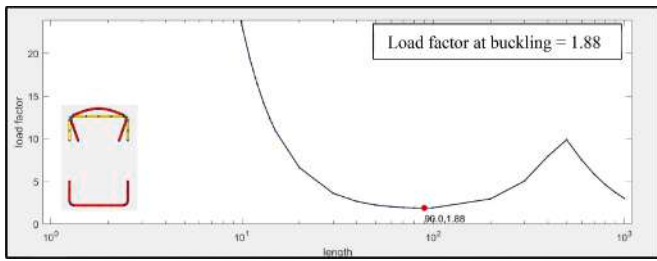


Fig. 12. CUFSM calculation results for specimen L120x80x3D50T300.

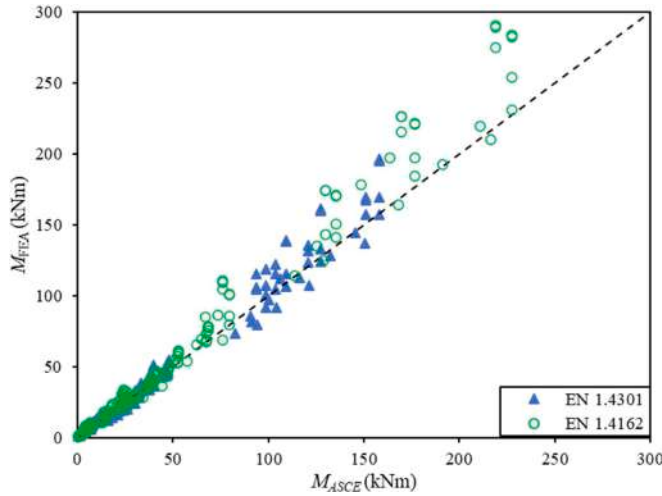


Fig. 13. Comparison of nominal flexural strengths obtained from FEA and ASCE [18] at various temperatures.

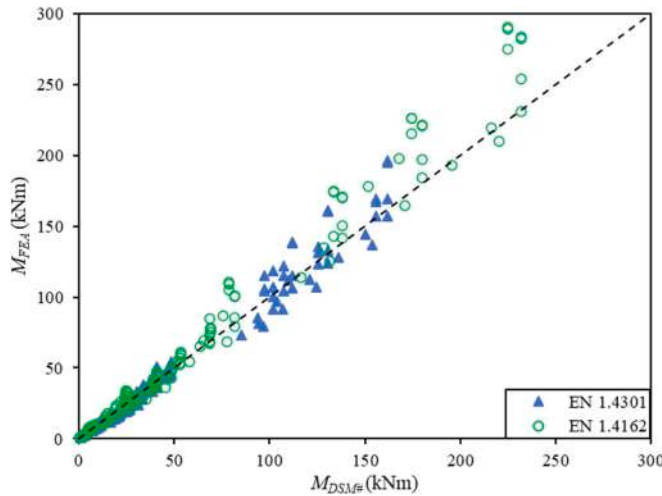


Fig. 14. Comparison of nominal flexural strengths obtained from FEA and modified DSM equations [22] at various temperatures.

1" was zero. Moreover, there were only 3% of sections with a web hole had $M_{FEA}/M_{EC3} < 1$ for the two grades of SS. The smallest value of M_{FEA}/M_{EC3} for the perforated sections was 0.94, according to Table 6. Thus, EC3 Part 1.4 [19] is considered to be reliable and safe.

5.6. EC3 part 1.2

The flexural strength obtained from EC3 Part 1.2 [13] ($M_{EC3\#}$) was determined using a similar approach to determine the M_{EC3} . The

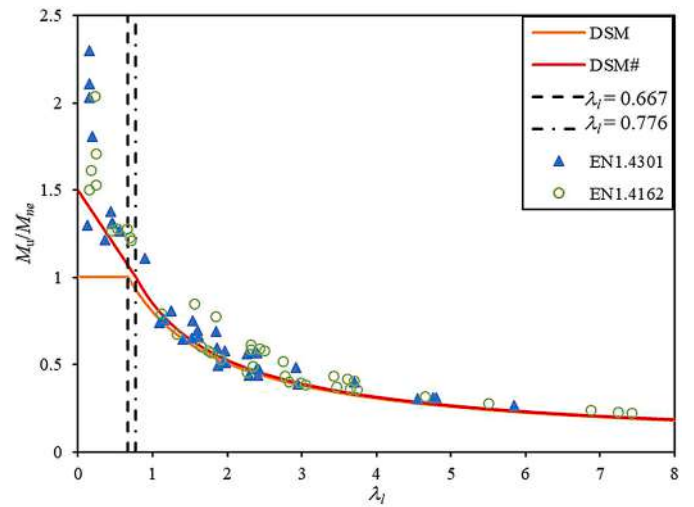


Fig. 15. Normalised FEA strength of specimens without a web hole with M_{ne} plotted against DSM (ASCE [18]) and modified DSM curves (DSM#).

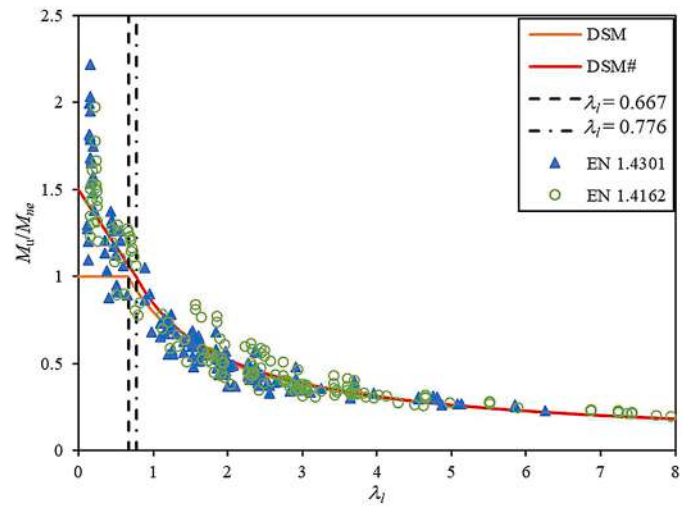


Fig. 16. Normalised FEA strength of perforated specimens with M_{ne} plotted against DSM (ASCE [18]) and modified DSM curves (DSM#).

cross-section classification and the effective section properties were calculated based on the material properties at ambient temperature, consistent with the rules prescribed in EC3 Part 1.2 [13]. The yield strength limit for $M_{EC3\#}$ was defined as $\sigma_{0.2}$ multiplied by the reduction factor $k_{y,T}$. The value of $k_{y,T}$ was the ratio between $\sigma_{0.2,T}$ and $\sigma_{0.2}$ for Class 4 sections and the ratio between $\sigma_{2.0,T}$ (elevated temperature strength at 2% strain) and $\sigma_{0.2}$ for Class 1 to 3 sections. The flexural strength equations, according to the above explanations, are shown in Eqs (15)-(17).

$$M_{EC3\#} = k_{y,T} S_e \sigma_{0.2} \quad (\text{for Class 4 cross - sections}) \quad (15)$$

$$M_{EC3\#} = k_{y,T} S_f \sigma_{0.2} \quad (\text{for Class 3 cross - sections}) \quad (16)$$

$$M_{EC3\#} = k_{y,T} Z \sigma_{0.2} \quad (\text{for Class 1 or 2 cross - sections}) \quad (17)$$

The comparison between M_{FEA} and $M_{EC3\#}$ values is shown in Fig. 19, which shows that the M_{FEA} values are generally larger than $M_{EC3\#}$ at values above 50 kNm. The mean and COV values of $M_{FEA}/M_{EC3\#}$ are shown in Tables 5 and 6 for the specimens with and without a web hole, respectively. The design rules in EC3 Part 1.2 [13] were more conservative than those in EC3 Part 1.4 [19], with the mean values ranging

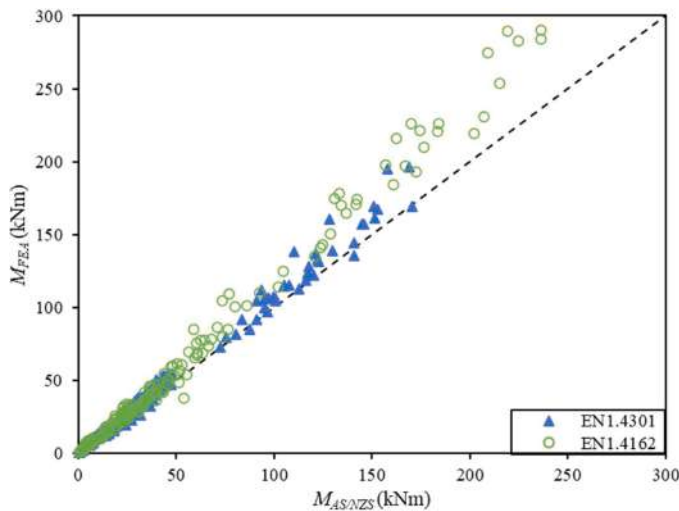


Fig. 17. Comparison of nominal flexural strengths obtained from FEA and AS/NZS [20] at various temperatures.

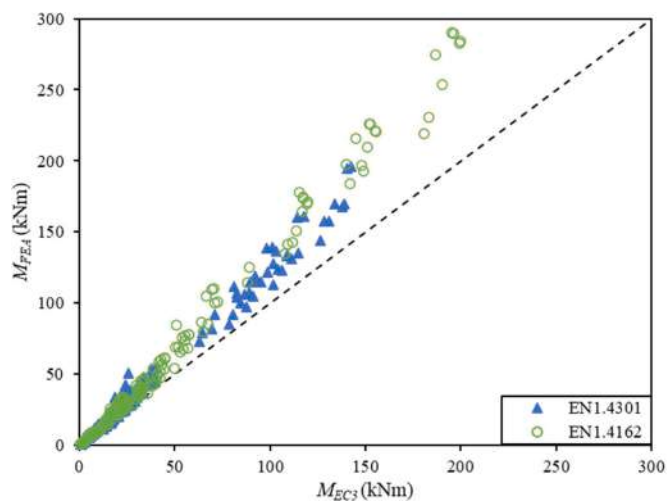


Fig. 18. Comparison of nominal flexural strengths obtained from FEA and EC3 Part 1.4 [19] at various temperatures.

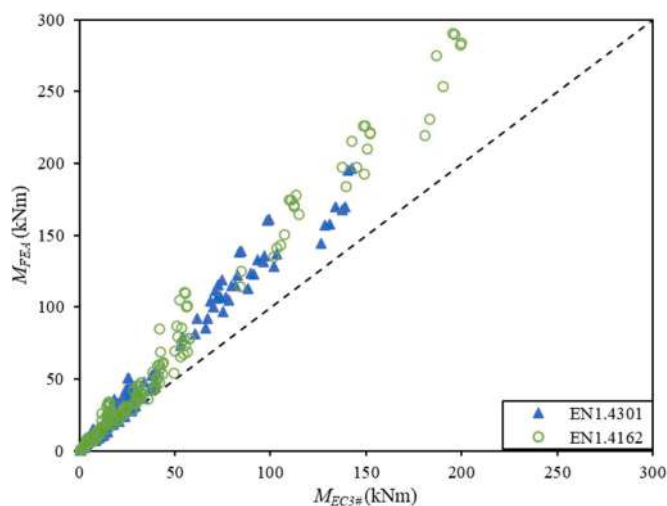


Fig. 19. Comparison of nominal flexural strengths obtained from FEA and EC3 Part 1.2 [13] at various temperatures.

from 1.34 to 1.43. The design rules in EC3 Part 1.2 [13] also produced relatively more scattered predictions than EC3 Part 1.4 [19], with the COV values ranging from 0.189 to 0.213. It is further shown in Table 5 and Table 6 that the EC3 Part 1.2 [13] design predictions were reliable for the sections with and without a web hole regardless of the grades of SS, as there is no β_0 value smaller than 2.5. Moreover, the design rules fulfilled the safety criteria according to the assessment proposed by Kruppa [26] since the design rules met the three safety criteria. Overall, the EC3 Part 1.2 [13] design rules offered the most conservative strength predictions for cold-formed SS beams with and without a web hole at elevated temperatures.

6. Conclusions

A numerical investigation for the flexural strength of cold-formed stainless steel RHS beams having various web hole sizes was conducted in this study. The investigation was based on a validated numerical model and an extensive parametric study. Four hundred numerical specimens with variations in cross-section size, yield strength, hole diameter and elevated temperatures were analysed using finite element (FE) method for the parametric study. The material properties of the FE model were generated from the recommendations of the previous studies [11,14]. Results from the FE analysis were used to evaluate the reliability and the safety of current flexural strength design rules recommended by ASCE [18], Chen et al. [22], AS/NZS [20], EC3 Part 1.4 [19], and EC3 Part 1.2 [13]. It should be noted that only the EC3 Part 1.2 [13] is specifically for the structural design at elevated temperatures. The flexural strengths predicted from the EC3 Part 1.2 [13] were based on the reduction factors of yield strength at elevated temperatures, while the strengths predicted by the other specifications were based on reduced yield strength due to elevated temperatures.

The strengths predicted by all design rules were conservative for the RHS beams with various hole diameters fabricated from austenitic and lean duplex stainless steel simulated at elevated temperatures. The most conservative strength predictions were provided by the design rules recommended by EC3 Part 1.2 [13]. However, the least scattered predictions were offered by EC3 Part 1–4 [19], as the COV values of numerical to nominal predicted strength ratio were generally the lowest amongst the other design rules. Furthermore, reliability analysis was carried out based on the available statistical parameters. The results showed that only the EC3 Part 1.4 [19] and EC3 Part 1.2 [13] design rules could achieve a minimum reliability index of 2.5 for predicting the flexural strengths of the RHS beams with and without a web hole. The safety assessment using the three criteria for structures at elevated temperatures proposed by Kruppa [26] was also performed. Again, both EC3 [19,13] design rules which were based on effective section properties could meet the three criteria.

Based on the two reliability analyses, the flexural strength design rules using DSM equations in the ASCE [18] was reliable for sections without a web hole at elevated temperatures, but not reliable for sections with a web hole. However, the strength predictions using the modified DSM equations proposed by Chen et al. [22] were not reliable for sections with and without a web hole based on Kruppa’s criteria. On the other hand, the design rules using effective width approach in the AS/NZS [20] was reliable for sections with a web hole, but not reliable for sections without a web hole.

CRediT authorship contribution statement

Andy Prabowo: Conceptualization, Methodology, Validation, Formal analysis, Investigation, Writing – original draft. **Yuner Huang:** Conceptualization, Methodology, Writing – review & editing. **Ben Young:** Conceptualization, Writing – review & editing, Supervision, Project administration.

Declaration of Competing Interest

The authors declare that they have no known competing financial interests or personal relationships that could have appeared to influence the work reported in this paper.

Data availability

Data will be made available on request.

Acknowledgements

The authors would like to acknowledge the Directorate of Research and Community Services of Universitas Tarumanagara Indonesia for providing the internal research grant for this research. The authors are grateful to Mr Kelsen Andrian Priestley and Mr Jonathan for contributing to this research as part of their final year undergraduate project. The computations were performed using research computing facilities provided by Tarumanagara Foundation, Indonesia.

References

- [1] K.A. Cashell, N.R. Baddoo, Ferritic stainless steels in structural applications, *Thin Walled Struct.* 83 (C) (2014) 169–181.
- [2] N.R. Baddoo, P. Francis, Development of design rules in the AISC Design Guide for structural stainless steel, *Thin Walled Struct.* 84 (2014) 393–405.
- [3] Y. Huang, J. Chen, Y. He, B. Young, Design of cold-formed stainless steel RHS and SHS beam–columns at elevated temperatures, *Thin Walled Struct.* 165 (2021), 107960.
- [4] Y. Huang, B. Young, Structural performance of cold-formed lean duplex stainless steel beams at elevated temperatures, *Thin Walled Struct.* 129 (2018) 20–27.
- [5] Y. Huang, B. Young, Finite element analysis of cold-formed lean duplex stainless steel columns at elevated temperatures, *Thin Walled Struct.* 143 (2019), 106203.
- [6] X. Yan, T. Gernay, Local buckling of cold-formed high-strength steel hollow section columns at elevated temperatures, *J. Constr. Steel Res.* 196 (2022), 107403.
- [7] Z. Xing, O. Zhao, M. Kucukler, L. Gardner, Testing of stainless steel I-section columns in fire, *Eng. Struct.* 227 (2021) 11320.
- [8] C. Quan, M. Kucukler, Simulation and cross-section resistance of stainless steel SHS and RHS at elevated temperatures, *Thin Walled Struct.* 189 (110849) (2023).
- [9] Z. Xing, M. Kucukler, L. Gardner, Local buckling of stainless steel plates in fire, *Thin Walled Struct.* 148 (106570) (2020).
- [10] Z. Xing, M. Kucukler, L. Gardner, Local buckling of stainless steel I-sections in fire: finite element modelling and design, *Thin Walled Struct.* 161 (107486) (2021).
- [11] J. Chen, B. Young, Stress–strain curves for stainless steel at elevated temperatures, *Eng. Struct.* 28 (2006) 229–239.
- [12] L. Gardner, A. Insausti, K. Ng, M. Ashraf, Elevated temperature material properties of stainless steel alloys, *J. Constr. Steel Res.* 66 (2010) 634–647. 66.
- [13] EC3, Design of Steel Structures — Part 1-2: General rules — Structural fire design. BS EN 1993-1-2:2005, European Committee for Standardization (EC3), Brussels, Belgium, 2010.
- [14] Y. Huang, B. Young, Stress–strain relationship of cold-formed lean duplex stainless steel at elevated temperatures, *J. Constr. Steel Res.* 92 (2014) 103–113.
- [15] S. Fan, L. Jia, X. Lyu, W. Sun, M. Chen, J. Zheng, Experimental investigation of austenitic stainless steel material at elevated temperatures, *Constr. Build. Mater.* 155 (2017) 267–285.
- [16] S. Fan, R. Ding, J. Zheng, F. Xie, Q. Wu, Refined model for the stress-strain curve of austenitic stainless-steel materials at elevated temperatures, *J. Struct. Eng.* 32 (4) (2020), 04020032.
- [17] W.W. Yu, R.A. LaBoube, H. Chen, *Cold-formed Steel Design (Fifth Ed.)*, Fifth ed., John Wiley & Sons, Inc., Hoboken, New Jersey, 2020.
- [18] ASCE, Specification For the Design of Cold-Formed Stainless Steel Structural members. SEL/ASCE8-22, American Society of Civil Engineers, Reston, Virginia, 2022.
- [19] EC3, Design of Steel Structures — Part 1.4: General rules—Supplementary Rules For Stainless steels. BS EN 1993-1-4:2006+A2:2020, European Committee for Standardization (EC3), Brussels, Belgium, 2020.
- [20] AS/NZS, Cold-formed Stainless Steel structures. AS/NZS 4673:2001, Standards Australia/Standards New Zealand, Sydney, NSW, 2001.
- [21] AISI, North American Specification For the Design of Cold-Formed Steel Structural members. AISI S100-16, American Iron and Steel Institute, Washington D.C., 2016.
- [22] Z. Chen, Y. Huang, B. Young, Design of cold-formed ferritic stainless steel RHS perforated beams, *Eng. Struct.* 250 (2022), 113372.
- [23] R. Feng, W. Sun, C. Shen, J. Zhu, Experimental investigation of aluminum square and rectangular beams with circular perforations, *Eng. Struct.* 151 (2017) 613–632.
- [24] ABAQUS, *Standard user's manual*, Dassault Systèmes Simulia Corp, 2023.
- [25] T.M. Chan, L. Gardner, Bending strength of hot-rolled elliptical hollow sections, *J. Constr. Steel Res.* 64 (2008) 971–986.
- [26] J. Kruppa, Eurocode fire parts: proposal for a methodology to check the accuracy of assessment methods. CEN TC 250, Horizontal Group Fire, 1999, pp. 99–130.
- [27] V.Z. Meimand, B.W. Schafer, Impact of load combinations on structural reliability determined from testing cold-formed steel components, *Struct. Saf.* 48 (2014) 25–32.
- [28] B.W. Schafer, S. Adány, Buckling analysis of cold-formed steel members using CUPSM: conventional and constrained finite strip methods, in: Eighteenth international specialty conference on cold-formed steel structures, Orlando, Florida, 2006.
- [29] C.D. Moen, B.W. Schafer, Extending Direct Strength Design to Cold-formed Steel Beams with Holes, in: International Specialty Conference on Cold-Formed Steel Structures. 4, St. Louis, Missouri, 2010.
- [30] EC3, Design of Steel Structures — Part 1-5: Plated structural elements. BS EN 1993-1-5:2006+A2:2019, European Committee for Standardization (EC3), Brussels, Belgium, 2019.